

3D Velocity Field and Flow Profile Reconstruction from Arbitrarily Sampled Doppler Ultrasound Data

Oliver Zettinig*, Christoph Hennemersperger*, Christian Schulte zu Berge,
Maximilian Baust, and Nassir Navab

Computer Aided Medical Procedures, Technische Universität München, Germany
oliver.zettinig@tum.de

Abstract. With the need for adequate analysis of blood flow dynamics, different imaging modalities have been developed to measure varying blood velocities over time. Due to its numerous advantages, Doppler ultrasound sonography remains one of the most widely used techniques in clinical routine, but requires additional preprocessing to recover 3D velocity information. Despite great progress in the last years, recent approaches do not jointly consider spatial and temporal variation in blood flow. In this work, we present a novel gating- and compounding-free method to simultaneously reconstruct a 3D velocity field and a temporal flow profile from arbitrarily sampled Doppler ultrasound measurements obtained from multiple directions. Based on a laminar flow assumption, a patch-wise B-spline formulation of blood velocity is coupled for the first time with a global waveform model acting as temporal regularization. We evaluated our method on three virtual phantom datasets, demonstrating robustness in terms of noise, angle between measurements and data sparsity, and applied it successfully to five real case datasets of carotid artery examination.

1 Introduction

Today, there are several medical imaging techniques for non-invasive quantitative and qualitative blood flow assessment. Although conventional Doppler ultrasound (US) sonography suffers from limited anatomical accessibility as well as high inter-observer variability, it is still an indispensable imaging modality for this task in clinical routine. The reason for this fact is that in comparison to 4D magnetic resonance imaging and digital subtraction angiography, US is broadly available, allows for fast acquisitions, offers high frame rates, and does not expose the patient to ionizing radiation or nephrotoxic contrast agent. Yet, Doppler US can only measure the projection of the true velocity vector along the echo beam direction and is thus blind to the flow orthogonal to it. As a consequence, examiners need experience in order to make qualitative assertions regarding the

* These authors contributed equally to this work.

three-dimensional blood flow, which also explains the recent endeavors to reconstruct three-dimensional flow fields from multiple Doppler acquisitions.

Since the early works by Fox et al. [1], who utilized simultaneous measurements from multiple directions to recover velocity information, cross-beam techniques have been proposed to overcome this limitation [2]. Alternative approaches such as the augmentation of single 2D Doppler images using ventricular wall motion [3] have the potential to successfully reconstruct vortex patterns but rely on additional restrictions. Arigovindan et al. [4] introduced B-spline grids to regularize the reconstruction problem. An extension of their approach by Gomez et al. [5] allows for 3D blood flow quantification from multiple registered B-Mode and Doppler volumes acquired by a 2D matrix array probe. However, the method requires pulse phase consistency, i.e. samples acquired at (or interpolated for) the same instant in time, and fails if temporally arbitrary Doppler samples are used. Inspired by the work of Waechter et al. [6], who employ a waveform model to regularize the estimation of blood flow parameters from rotational angiography, we propose a method which facilitates the simultaneous reconstruction of both a continuous three-dimensional velocity field and a continuous waveform model. Thanks to the temporal regularization provided by the waveform model, the proposed method is *gating-free* in the sense that no data selection according to a gating signal is required and that the reconstruction is performed over the entire dataset at once. Therefore, it supports temporally arbitrary Doppler samples from any pulse phase as input. Moreover, the proposed approach is also *compounding-free* as it is based on the raw Doppler in-phase and quadrature (IQ) samples and thus also allows spatially arbitrary, non-uniform data points, without prior compounding of US volumes and associated interpolation artifacts.

2 Methods

The reconstruction method relies on raw Doppler IQ samples as input. In particular, 4-tuples of $(\mathbf{p}, \mathbf{d}, m, t)$ are collected for every sample, where $\mathbf{p} = [p_x, p_y, p_z]^\top$ denotes the sample position in Cartesian space, \mathbf{d} the corresponding normalized echo beam direction, m the measured Doppler signal, and $t \in [0, 1]$ the normalized pulse phase time. B-spline basis functions are employed to describe a smooth 3D velocity field $\mathbf{v}(\mathbf{p}) = [v_x(\mathbf{p}), v_y(\mathbf{p}), v_z(\mathbf{p})]^\top$ [5], whose components are given by

$$v_\gamma(\mathbf{p}) = \sum_{i,j,k} c_{i,j,k}^\gamma \beta_{s,i}^n(p_x) \beta_{s,j}^n(p_y) \beta_{s,k}^n(p_z), \quad \text{for } \gamma \in \{x, y, z\}. \quad (1)$$

The indices i , j , and k indicate a location in the regular, three-dimensional B-spline grid with spacing s , which defines the resolution of the recovered vector field. $\beta_{s,i}^n(p_x) = \beta^n(i/s - p_x)$ denotes the scaled and translated B-spline basis function of degree n at grid position i , likewise for $\beta_{s,j}^n(p_y)$ and $\beta_{s,k}^n(p_z)$. Finally, $c_{i,j,k}^\gamma$ are the corresponding B-spline coefficients to be found.

The original approach in [5] relies on an input dataset with N samples sharing the same pulse phase, from which the reconstruction is performed by minimizing

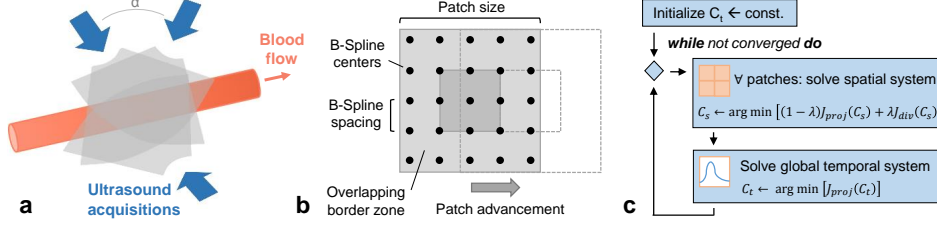


Fig. 1: **a)** Three ultrasound sweeps from different directions are necessary to reconstruct the velocity field in a blood vessel. **b)** Illustration of the patch-wise reconstruction scheme. After reconstruction, only the estimated B-spline coefficients in the non-overlapping core zone are stored. **c)** Algorithm to solve spatial velocity field and temporal flow profile function. *See text for details.*

the error between the measured Doppler value denoted by m_r and the projection of the recovered velocity at sample position \mathbf{p}_r onto the beam direction \mathbf{d}_r .

$$J_{proj}(\mathbf{v}) = \sum_{r=1}^N \|\mathbf{d}_r \cdot \mathbf{v}(\mathbf{p}_r) - m_r\|_2^2. \quad (2)$$

However, this formulation has to be adjusted for different pulse phases because the blood flow at every point within an artery varies over time. Thus, uncorrected Doppler measurements lead to inconsistent samples, prohibiting the reconstruction of the velocity field at a given instant. In this work, we introduce a flow profile function $\varphi(t): [0, 1] \rightarrow [0, 1]$ mapping from normalized pulse phase times to scaling factors compensating the varying flow patterns (Fig. 2a). The actual velocity vector at any point in time is then given by $\mathbf{v}(\mathbf{p}, t) = \varphi(t) \mathbf{v}_{max}(\mathbf{p})$, assuming a pulsatile laminar flow. While allowing varying velocity magnitudes over time, our formulation keeps the flow direction constant at any position in the reconstructed volume. Unless bifurcations, high-grade stenoses, or aneurysms are investigated, this model has been shown to introduce only negligible errors [6]. It should be noted, however, that this formulation does not enforce the velocity directions to be organized in parallel sheets. In order to compute φ , we employ a B-spline parametrization as well: $\varphi(t) = \sum_{\xi=1}^T c_{\xi}^t \beta_{\tau, \xi}^n(t)$, where $\beta_{\tau, \xi}^n(t)$ is a periodic B-spline basis function of degree n and spacing τ evaluated at grid point ξ , and c_{ξ}^t denote the corresponding temporal B-spline coefficients. As a result, we propose the cost function

$$J_{proj}(\mathbf{v}, \varphi) = \sum_{r=1}^N \|\varphi(t_r) \mathbf{d}_r \cdot \mathbf{v}_{max}(\mathbf{p}_r) - m_r\|_2^2 \quad \text{s.t.} \quad \max_t |\varphi(t)| = 1 \quad (3)$$

The constraint in Eq. 3 is added to the system to ensure that \mathbf{v}_{max} is correctly scaled. For a matrix form expression, the spatial B-spline coefficients are gathered in vector $\mathbf{C}_s = \{c_{i,j,k}^x, c_{i,j,k}^y, c_{i,j,k}^z\}$, the temporal ones in vector $\mathbf{C}_t = \{c_{\xi}^t\}$. The evaluation of the B-spline functions is encoded, after vectorization of the 3D

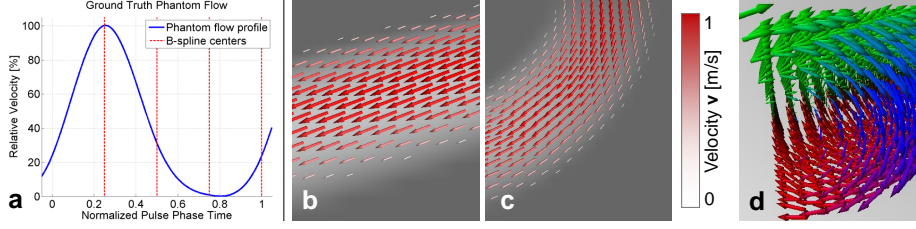


Fig. 2: **a)** Ground truth flow profile function defined using periodic B-spline coefficients. **b-d)** Results of phantom experiment reconstructions closely reflect expected results. Vector fields for *Linear* (b) and *Curved* (c) phantoms, as visible in longitudinal slices, follow vessel direction indicated in the background and exhibit quadratic velocity distributions. Expected rotatory symmetry in the *Barrel Roll* phantom (d) can be easily observed using direction-based color-mapping.

spatial grid of size M , by sampling matrices $\mathbf{S}_s \in \mathbb{R}^{3N \times 3M}$ and $\mathbf{S}_t \in \mathbb{R}^{N \times T}$

$$\mathbf{S}_s = \begin{bmatrix} S_p & 0 & 0 \\ 0 & S_p & 0 \\ 0 & 0 & S_p \end{bmatrix} \quad \text{with} \quad \begin{cases} \{S_p\}_{r, \text{vec}(i,j,k)} = \beta_{s,i}^n(p_{r,x})\beta_{s,j}^n(p_{r,y})\beta_{s,k}^n(p_{r,z}), \\ \text{and} \quad \{S_t\}_{r,\xi} = \beta_{\tau,\xi}^n(t) \end{cases} \quad (4)$$

such that $\mathbf{v}_{max} = \mathbf{S}_s \mathbf{C}_s$ and $\varphi = \mathbf{S}_t \mathbf{C}_t$. The dot product is realized using the direction matrix $\mathbf{D} = [\mathbf{D}^x \mathbf{D}^y \mathbf{D}^z]$ containing diagonal matrices with the three Cartesian components of the beam directions, respectively: $\{\mathbf{D}^x\}_{r,r} = d_{x,r}$, likewise for \mathbf{D}^y and \mathbf{D}^z . With $\mathbf{m} = \{m_i\}$ referring to the vector of Doppler measurements and \otimes to the component-wise multiplication, the cost function reads

$$J_{proj}(\mathbf{C}_s, \mathbf{C}_t) = \|(\mathbf{S}_t \mathbf{C}_t) \otimes (\mathbf{D} \mathbf{S}_s \mathbf{C}_s) - \mathbf{m}\|_2^2. \quad (5)$$

For smoothness, a spatial regularization term is added to the final cost function:

$$J(\mathbf{C}_s, \mathbf{C}_t) = (1 - \lambda) J_{proj}(\mathbf{C}_s, \mathbf{C}_t) + \lambda J_{div}(\mathbf{C}_s). \quad (6)$$

As shown in [5], the locally acting divergence term $J_{div} = \|\nabla \cdot \mathbf{v}_{max}\|_2^2$, derived using the B-spline formulation, enforces the incompressibility of the blood flow. It should be noted that the flow profile function φ inherently acts as temporal regularization itself, rendering further regularization terms unnecessary.

Provided a global flow profile function φ , the velocity field \mathbf{v}_{max} can be reconstructed directly in a patch-wise fashion. Simultaneously solving for both \mathbf{v}_{max} and φ is, however, not possible. Instead, spatial and temporal coefficients are obtained in an alternating fashion as reported in Fig. 1c. We employ a LU decomposition with partial pivoting to directly solve the patch-wise spatial system. Hereby, patches mutually overlap for increased stability, and only the core, non-overlapping coefficients in vector \mathbf{C}_s are stored (Fig. 1b). The global temporal coefficients \mathbf{C}_t are found using a Levenberg-Marquardt solver. Eventually, the algorithm yields two continuously defined results: the reconstructed maximum velocity field \mathbf{v}_{max} and the blood flow profile φ .

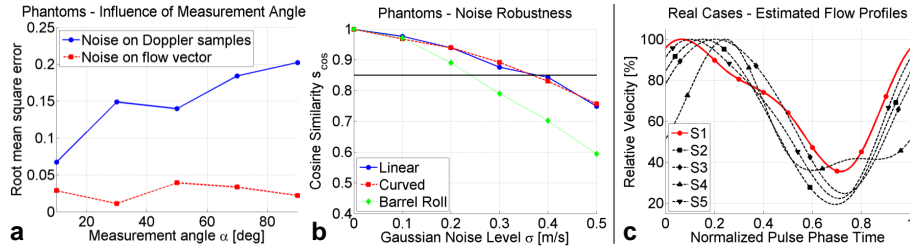


Fig. 3: **a)** The counterintuitive relation between α and the root mean squared error is only present if noise is directly applied to the Doppler samples, regardless of the direction of acquisition. **b)** Gaussian noise of up to $\sigma \leq 0.35$ m/s (*Linear* and *Curved* phantoms) can be added to the Doppler samples before the cosine similarity s_{cos} drops below the success threshold. **c)** The estimated flow profiles of all five subjects reveal the pulsatility of the artery. See text for details.

3 Experiments

Phantom Evaluation. For evaluating our method, three virtual phantom datasets, each spanning $34 \times 34 \times 34$ mm, were created. The first two phantoms, denoted *Linear* and *Curved*, contained a cylinder and a torus with a vessel radius of 6 mm, respectively. A quadratic Poiseuille flow with a velocity of $\mathbf{v}_{max,ph} = 1$ m/s in the centerline was applied. The velocity for the third phantom, denoted *Barrel Roll*, was defined as $\mathbf{v}(\mathbf{p}) = a[\mathbf{p} - \mathbf{r}(\mathbf{r} \cdot \mathbf{p})] \times \mathbf{r}$, where \mathbf{r} is the direction of the roll and a a scaling factor to ensure $\max \mathbf{v}_{max,ph} = 1$ [7]. In all cases, a phantom flow profile function φ_{ph} as shown in Fig. 2a was used to construct a time-varying flow profile. Finally, synthetic Doppler sweeps from three directions \mathbf{d} were generated with in total N measurements $m = \varphi_{ph}(t \sim [0, 1]) \mathbf{d} \cdot \mathbf{v}_{max,ph}(\mathbf{p}) + \eta_s + \eta_v$. The pairwise angle between the sweeps, denoted opening angle α as illustrated in Fig. 1a, was varied between 10° and 90° . For the linear phantom, the mean direction \mathbf{d} was set to be 45° tilted against the vessel direction. Two different Gaussian noise models were considered: On the one hand, noise with standard deviation σ was added to the samples such that $\eta_s = \mathcal{N}(0, \sigma)$ simulated inaccuracies of the Doppler measurement itself. On the other hand, noise added to the velocity vector under investigation such that $\eta_v = \vec{\mathbf{v}} \cdot \mathbf{d} \mathcal{N}(0, \sigma)$, with $\vec{\mathbf{v}} = \mathbf{v} / \|\mathbf{v}\|$, modeled inaccuracies of the tracking system or badly synchronized temporal data. The sample positions \mathbf{p} were chosen from a regular grid with 1 mm spacing. Pulse phase times t were randomly drawn from a uniform distribution. The reconstruction was performed using $6 \times 6 \times 6$ mm patches, with 2 mm overlap, for which only ρN samples were used to mimic sparse sampling (data density $\rho \in [0.6, 1]$). The spatial spacing of the cubic B-splines was fixed at $s = 1.5$ mm. Due to the high runtime complexity of the alternating algorithm (Fig. 1c), a coarse temporal spacing of $\tau = 0.25$ was used. For all experiments, moderate regularization ($\lambda = 0.1$) and cubic B-splines ($n = 3$) were employed. Three measures were used to analyze reconstruction errors of computed velocities $\mathbf{v}_{max,c}$ and the estimated flow profile φ_c . While the mean cosine similarity s_{cos} and the mean Euclidean norm e_d quantify errors of the velocity field, the

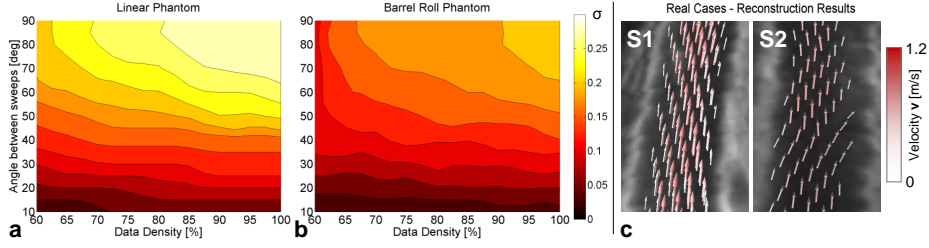


Fig. 4: **a-b)** Maximum tolerable Gaussian noise level σ for linear and barrel roll phantoms such that reconstructions fulfill $s_{cos} > 0.85$ and $e_d < 0.15$. More noise (up to $\sigma = 0.25$ m/s) can be added to samples with higher data density and higher angles between sweeps to still obtain successful reconstructions.

c) Carotid artery reconstruction results for two exemplary subjects. Overlay of velocity fields on longitudinal B-mode image slices. *See text for details.*

root mean squared error e_{rms} measures how well the flow profile was recovered:

$$\begin{aligned}
 s_{cos} &= \frac{1}{N} \sum_{r=1}^N \vec{\mathbf{v}}_{max,c}(\mathbf{p}_r) \cdot \vec{\mathbf{v}}_{max,ph}(\mathbf{p}_r), \\
 e_d &= \frac{1}{N} \sum_{r=1}^N \|\mathbf{v}_{max,c}(\mathbf{p}_r) - \mathbf{v}_{max,ph}(\mathbf{p}_r)\|_2, \\
 e_{rms} &= \sqrt{\frac{1}{N} \sum_{r=1}^N [\varphi_c(t_r) - \varphi_{ph}(t_r)]^2}.
 \end{aligned} \tag{7}$$

Real Case Acquisition and Preprocessing Protocol. We tested our method on five carotid artery screening datasets of 25 - 31 year old subjects. An open access ultrasound system (Aurotech ultrasound AS, model MANUS) with a linear array probe (128 elements, single element width 0.27 mm, height 4 mm, focal depth 30 mm, 45 aperture elements) operating at 8 MHz, was used together with an electromagnetic (EM) tracking system (Ascension Technology Corporation, model TrakStar) and a pulse-oximetry sensor (Medlab GmbH, model P-OX100). After calibration and preprocessing as described in [8], the system facilitates the acquisition of Doppler IQ samples as well as a normalized pulse phase signal, mapping the peak-to-peak distances to a linear signal in the interval $[0, 1]$. For each subject, three US sweeps, mutually around $\alpha = 60^\circ$ apart, were acquired. To correct for the limited precision of the EM tracking system, the Doppler magnitudes of each sweep were manually thresholded to obtain a point cloud of the blood vessel. The three point clouds were then registered using ICP in a pairwise manner. It should be noted that a sufficiently precise tracking system, e.g. mechanical tracking, would make this preprocessing obsolete.

4 Results and Discussion

Phantom Experiments. Fig. 2b-d illustrate reconstruction results for all phantoms with the ideal parameter configuration $\alpha = 90^\circ$, $\eta_s = \eta_v = 0$, and $\rho = 1$. For the estimation of the flow profile, the correlation r between e_{rms} and the

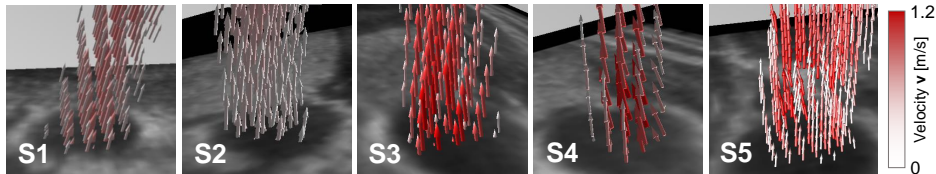


Fig. 5: **Carotid artery reconstruction results** for all five subjects. Overlay of velocity fields on cross-sectional B-mode image slices illustrate that the blood flow pattern was qualitatively well captured (*compounding only for reference*).

acquisition parameters was investigated. Interestingly, increasing opening angles α led to higher errors ($r_{rms,\alpha} = +0.18$) when only η_s was applied, which is intuitively more likely to cancel out if all samples are roughly obtained from one direction ($\alpha \approx 0^\circ$). If, however, only η_v was used, no significant relationship between angle and error could be observed ($r_{rms,\alpha} = -0.03$), as shown in Fig. 3a. Although we expect the latter noise model to be dominant in a clinical scenario, the former model facilitates evaluating the limitations of the method. Therefore, we set $\eta_v = 0$ for all subsequent experiments.

A reconstruction of the velocity field was considered successful if $s_{cos} \geq 0.85$ and $e_d \leq 0.15$ mm. As shown in Fig. 3b, Gaussian noise of up to $\sigma \leq 0.35$ m/s could be added to the Doppler samples under ideal measurement conditions of $\alpha = 90^\circ$ and $\rho = 1$, before the cosine similarity s_{cos} dropped below the success threshold (similar results were obtained for the Euclidean norm e_d). We evaluated the effect of data density and angle between the measurements for the same noise range. Figure 4a-b illustrate the maximum tolerable noise level σ for various acquisition parameters, indicating robustness in terms of data sparsity. As expected, the method was most sensitive to noise for the vortex patterns of the *Barrel Roll* phantom.

Real Case Evaluation. Despite the coarse temporal grid spacing, realistic and qualitatively accurate velocity fields and flow profiles could be successfully reconstructed with a resolution of 1 mm for all five datasets. The estimated flow profiles captured the pulsatility of the artery well (Fig. 3c). Results illustrated in Fig. 4c and Fig. 5 show an overall promising agreement between vector fields and vessel anatomies as seen in the B-mode images. However, in some datasets, e.g. S2, reconstruction errors at the vessel borders are evident. While phantom experiments suggest an unsatisfactory registration of the three sweeps and thus missing vector information at the borders, further evaluation is necessary to assess the effect of the spatially relaxed laminarity assumption.

5 Conclusion and Future Work

In this work, we have presented a novel approach to quantify varying blood velocities over time from spatially and temporally arbitrarily sampled Doppler ultrasound measurements. For the first time and to the best of our knowledge,

we were able to simultaneously reconstruct a continuous three-dimensional blood velocity field and a periodic temporal flow profile function by coupling a patch-wise B-spline formulation of blood velocity with a waveform model. With the assumption of a laminar flow, our both gating- and compounding-free framework supports Doppler samples from any pulse phase acquired with a tracked free-hand ultrasound system. As presented on three virtual phantom datasets, our method is robust with respect to noise, angle between measurements and data sparsity. We were also able to present promising results on five real case datasets of carotid artery screening, showing qualitatively well captured blood flow patterns and realistic, pulsatile flow profiles. Apart from a potentially expedient diagnostic value in clinical routine, our approach may have further important applications, for instance as initialization of computational fluid dynamics models by the recovered flow profile. Possible future extensions of this work include a detailed parameter evaluation, a thorough quantitative validation, a more local definition of the flow profile for handling bifurcations, and an improvement of ultrasound sweep registration toward higher velocity field resolution.

Acknowledgements. This work was partially supported by the EU 7th Framework, No. 270460, and the Bavarian state program Leitprojekte Medizintechnik (BayMED).

References

- [1] Fox, M.D.: Multiple Crossed-beam Ultrasound Doppler Velocimetry. *Sonics and Ultrasonics, IEEE Transactions on* **25**(5) (1978) 281–286
- [2] Dumire, B., Beach, K., Labs, K., Plett, M., Strandness Jr, D.: Cross-beam Vector Doppler Ultrasound for Angle-independent Velocity Measurements. *Ultrasound in Medicine & Biology* **26**(8) (2000) 1213–1235
- [3] Garcia, D., del Álamo, J.C., Tanné, D., Yotti, R., Cortina, C., Bertrand, É., Antoranz, J.C., Pérez-David, E., Rieu, R., Fernández-Avilés, F., et al.: Two-dimensional Intraventricular Flow Mapping by Digital Processing Conventional Color-Doppler Echocardiography Images. *Medical Imaging, IEEE Transactions on* **29**(10) (2010) 1701–1713
- [4] Arigovindan, M., Suhling, M., Jansen, C., Hunziker, P., Unser, M.: Full Motion and Flow Field Recovery from Echo Doppler Data. *Medical Imaging, IEEE Transactions on* **26**(1) (2007) 31–45
- [5] Gomez, A., Pushparajah, K., Simpson, J.M., Giese, D., Schaeffter, T., Penney, G.: A Sensitivity Analysis on 3D Velocity Reconstruction from Multiple Registered Echo Doppler Views. *Medical Image Analysis* **17**(6) (2013) 616–631
- [6] Waechter, I., Bredno, J., Hermans, R., Weese, J., Barratt, D.C., Hawkes, D.J.: Model-based Blood Flow Quantification from Rotational Angiography. *Medical Image Analysis* **12**(5) (2008) 586–602
- [7] Hastenteufel, M.: Neue Methoden des 3D Ultraschalls zur Geschwindigkeitsrekonstruktion und intraoperativen Navigation. PhD thesis, Universität Fridericiana, Karlsruhe, Germany (2005)
- [8] Hennersperger, C., Karamalis, A., Navab, N.: Vascular 3D+T Freehand Ultrasound using Correlation of Doppler and Pulse-Oximetry Data. In Stoyanov, D., Collins, D.L., Sakuma, I., Abolmaesumi, P., Jannin, P., eds.: *IPCAI 2014. LNCS. Volume 8498.*, Springer, Heidelberg (2014) in press.